Structural Monitoring and Maintenance, *Vol. 9, No. 1 (2022) 81-105*
https://doi.org/10.12989/smm.2022.9.1.081

Nonlinear numerical analysis and proposed equation for axial loading capacity of concrete filled steel tube column with initial imperfection

Haseeb Ahmad [1], Muhammad Fahad Ejaz [2] and Muhammad Aslam*[3]

[1] *FAST-National University of Computer and Emerging Sciences, 852 B Faisal Town, Lahore 54700, Pakistan*
[2] *Department of Civil Engineering and Environmental Engineering, Saitama University, Saitama, Japan*
[3] *Department of Civil Engineering, School of Engineering & Technology, Institute of Southern Punjab 60000 Multan, Pakistan*

(*Received September 17, 2021, Revised March 24, 2022, Accepted April 6, 2022*)

Abstract. The use of concrete filled steel tube (CFST) column is widely accepted due to its property of high axial load carrying capacity, more ductility and more resistant to earthquake specially using in bridges and high-rise buildings. The initial imperfection (δ) that produces during casting or fixing causes the reduction in load carrying capacity, this is the reason, experimental capacity is always less then theoretical one. In this research, the effect of δ on load carrying capacity and behavior of concrete filled steel tube (CFST) column have been investigated by numerically simulation of large number of models with different δ and other geometric parameters that include length (L), width (B), steel tube thickness (t), f_c' and f_y. Finite element analysis software ANSYS v18 is used to develop model of SCFST column to evaluate strength capacity, buckling and failure pattern of member which is applied during experimental study under cyclic axial loading. After validation of results, 42 models with different parameters are evaluated to develop empirical equation predicting axial load carrying capacity for different value of δ. Results indicate that empirical equation shows the 0 to 9% error for finite element analysis Forty-two models in comparison with ANSYS results, respectively. Empirical equation can be used for predicting the axial capacity of early estimating the axial capacity of SCFT column including δ.

Keywords: ANSYS; concrete filled steel tube column; finite element analysis; modelling; parametric study

1. Introduction

The growing desire of high load carrying capacity in addition with resistance to seismic activity compelled the researchers to study the composite columns like CFSTs. Studies of CFST column with different sections having high concrete strength including initial imperfections, compressive loads, bending and torsion have been conducted. To investigate the behavior of CFST column, the various full scale experimental researches were performed (Perea *et al*. 2013, Portolés *et al*. 2011a, Varma *et al*. 2002, Wei *et al*. 2020).

Total Eighteen full CFST columns were investigated and validate with advanced nonlinear fiber

*Corresponding author, Ph.D., Assistant Professor, E-mail: bhanbhroma@gmail.com

Copyright © 2022 Techno-Press, Ltd.
 ISSN: 2288-6605 (Print), 2288-6613 (Online)

analysis models by Perea *et al*. (2013). Outcomes related to pure axial compression accurately estimate strength and stiffness corresponding to current AISC provision. Simplified analytical method was introduced using experimental specimens to predicting ultimate strength of CFST column based on collapse theory with consideration of slight initial imperfection for investigation of moment magnification (Lu *et al*. 2007).

Wei *et al*. (2020) tested eighty-seven specimens of circular CFST short column with investigation parameters of diameter-to-thickness ratio (D/t), compressive strength (f_c') and yield strength of steel (F_y) and decreased with increase of (D/t). Exploration of results conclude that strength of CFST short column increased with increase of compressive strength (f_c') and yield strength of steel (F_y).

Six hollow and six solid CFST long columns was investigated to propose the unified analytical formulas for different sections. Researcher assumed the equivalent initial

imperfection directly proportional to steel ratio and stability factor of sections (Yu *et al*. 2010), also with different polygon sections (Yu *et al*. 2013). Researcher assumed the equivalent initial imperfection directly proportional to steel ratio and stability factor of sections.

The effect of material strength, diameter thickness ratio and axial compression ratio were analyzed in this study. CSFT columns with pure concrete and with reinforcing bars were considered by Li *et al*. (2018). Investigation showed that columns with reinforcing bars had high strength, toughness, more effective plastic behavior. To investigate the effect of normal strength concrete (NSC) and high strength concrete (HSC), Hernández-Figueirido *et al*. (2012) and Portolés *et al*. (2011b) performed tests on CFST columns provided with eccentricity. CSFT columns with NSC presented the more ductile response as compared to HSC but had less ability to perform under more axial load. Behavior of CFST column under self-consolidation ultra-high strength concrete (UHSC) with fiber reinforcement in it was investigated to improve ductility, fabrication and strength by Hossain *et al*. (2021). Schneider (1998) performed the fourteen tests, concluded circular concrete filled steel tube (CCFST) provides more confinement effect and post yield axial ductility. Varma *et al*. (2002) tested the eight SCFST column and concluded that Euro Code 4 overestimated the load capacity and AISC Code provide load capacity more conservative as compared to ACI Code.

Hundred and forty four specimens were tested by Sakino *et al*. (2004) concluded that increase in axial capacity was due to strain hardening of steel in square sample and in circular sample, was due to confinement. Jin *et al*. (2020) also carried out mesoscale simulation research to explore the effect of size and failure pattern of CFST column using lightweight aggregate under compression. Experimental and numerical investigation was conducted on effect of cross sectional shape of CFST column on overall response of column by Ayough *et al*. (2021). By using finite element modelling, design procedure was introduced using L-shaped and T-shaped CFST columns subjected to axial load and bending for parametric study by Liu *et al*. (2020).

Fiber analysis models was also used for CFST column for investigating axial capacity by Patel *et al*. (2017) and Liang *et al*. (2007). Song and Xiang (2020) performed FE analysis on structural behavior of ultra-high strength concrete (UHSC) and confined a new stress strain model for ultra-high strength concrete (UHSC). Similar, nonlinear finite element analysis was conducted by Ellobody *et al*. (2006) to evaluate the behavior of CFST column involving wide range of concrete strength of 30 MPa (NSC) to 110 MPa (HSC) and outer diameter of steel tube to thickness ratio (D/t).

Investigation was carried out by Nguyen *et al*. (2019), Hu *et al*. (2003) and He *et al*. (2019) to

analysis the confinement effect and buckling behavior of CFST columns. Results showed that CFST with circular and square section provide better confinement when (D/t < 40) and (B/t < 30), respectively. Effendi (2020) also performed experimental and numerical study to check response of concrete and steel interface and ultimate load carry capacity of CFST beam. Effect of impact load on CFST column was practiced by Du *et al*. (2019) experimentally and numerically, main parameter for conclusion was impact load, thickness, height of drop hammer and failure mode. Similarly, using same investigating parameters, recycled aggregates incorporated in concrete filled steel tube column was investigated to check axial load carrying capacity by Nour and Güneyisi (2019).

The semi analytical method was proposed by Lakshmi and Shanmugam (2002) to predict the behavior of CFST column. ANSYS was also used to predict the axial load capacity of CCSFT column by Gupta *et al*. (2012). The numerical modelling was practiced with CFST column subjected to eccentric loading by Portolés *et al*. (2011a) and Cai *et al*. (2020). Investigation was carried out to evaluate the overall buckling of the CFST columns with different concrete and steel strength, length, relative slenderness, width to thickness ratio (B/t) or diameter to thickness ratio (D/t) ratio.

Reinforced concrete columns retrofitted with different steel section were investigated and validate the finite element analysis using ANSYS by Belal *et al*. (2015) and found that 20% increase in load carrying capacity in case of angle section and C section. Finite element analysis software ANSYS was practiced by Wang and Li (2013) to study the failure mechanism of RC column under axial symmetrical and eccentric loading.

Eleven experimental geopolymer concrete filled steel tube columns with square and circular sections were investigated by applying compressive axial load with flexure loading. FEA validation and parametric study were conducted to develop safe design methodology (Fang and Visintin 2022).

The effect of axial compressive axial capacity, stiffness, and ductility of CFST columns are largely depended on material and geometric parameter which include initial imperfection produces during casting or fixing reduces the axial capacity of column. This research work is helpful to investigate actual response of CFST column subjected to various initial imperfections and predicting actual reduced load carrying capacity of member helping the optimization of structure. After verification of results, various models with different parameters are investigated to develop empirical equation predicting axial load carrying capacity against different initial imperfection.

2. Finite element modelling

ANSYS v18 (ANSYS User Manual Revision 18.0. 2018) is used in order to simulate accurate behavior of CFST, the following component of simulation as to be model properly. These

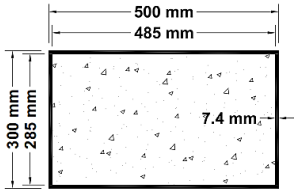

Fig. 1 Cross sectional view of experimental specimen

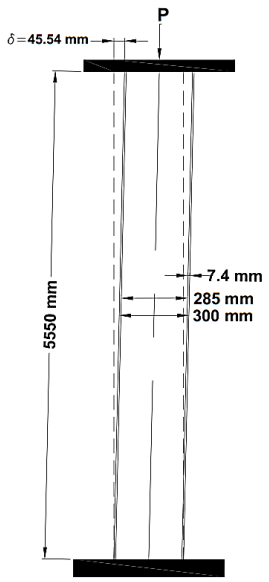

Fig. 2 Side view of experimental specimen

components are material model of steel and concrete, contact surface between steel and concrete elements and element types and meshing that have to be used for steel and concrete modelling. Figs. 1 and 2 show the cross-sectional and side view of experimental specimen called 8RW-18-12 as mentioned by Perea *et al.* (2013) respectively.

Table 1 represent the measured length (L), thickness of steel tube (t), initial imperfection (δ), concrete core size and overall size of column, and concrete compressive strength (f_c'), elastic modulus of concrete (E_c), yield strength of steel (f_y), ultimate strength of steel (f_u) and elastic modulus of steel (E_s) of experimental specimen called 8RW-18-12 as mentioned by Perea *et al*. (2013).

Table 1 Measured dimensions and material properties of experimental specimen

Dimensions	L (mm)	5550
	t (mm)	7.4
	δ (mm)	45.54
	Concrete core size (mm^2)	285 × 485
	Overall size (mm^2)	300 × 500
Material properties	f_c' (MPa)	87.6
	E_c (GPa)	41.9
	f_y (MPa)	365
	f_u (MPa)	502
	E_s (GPa)	202.4
Tested by Perea *et al*. (2013)		

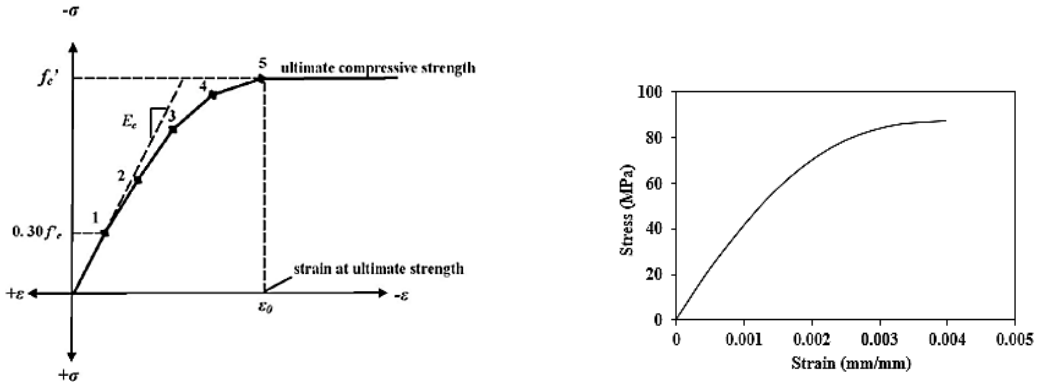

(a) Uniaxial stress strain curve of concrete (b) Calculated stress strain curve for concrete

Fig. 3 Stress strain curves of concrete

2.1 Material model

Concrete is brittle and has highly nonlinear relationship. Under the loading, nonlinear response attributed to formation and gradual growth of micro cracking. The range of tensile strength of concrete is typically 8-15% of compressive strength of concrete. The stress strain relationship curve of concrete in compression shows the linearly elastic behavior up to 30% of maximum compressive strength. Beyond this point, stress gradually increases and reaches to maximum compressive strength, softening region occurs and eventually crushing occurs at ultimate strain.

Fig. 3(a) shows the typical stress strain relationship curve for normal weight concrete. To simulate behavior of concrete, hognestad piecewise model is used. The curve starts at zero stress and strain. Point 1 is defined as 0.3 f_c', is calculated by linear behavior and must satisfy the Hooke's Law (Eq. (4)). Point 1, 2, 3 and 4 are calculated by (Eq. (2)) and $\varepsilon_\circ$ is obtained from (Eq. 3). The strains are calculated from above equations and then stresses are calculated against each strain. Point 5 represents the crushing strain at unconfined concrete corresponding to f_c' and $\varepsilon_\circ$. After that point, perfectly plastic behavior of concrete is assumed. Fig. 3(b) shows the calculated stress strain relationship used for this study in ANSYS v18 (ANSYS User Manual Revision 18.0. 2018) which is proposed by Kachlakev *et al*. (2001). Following equations are used to calculate multilinear stress strain behavior of concrete by Kachlakev *et al*. (2001).

$$E_c = 4700\sqrt{f_c'} \tag{1}$$

$$f = \frac{E_c\,\varepsilon}{1 + \left(\frac{\varepsilon}{\varepsilon_o}\right)^2} \tag{2}$$

$$\varepsilon_o = \frac{2f_c'}{E_c} \tag{3}$$

$$E_c = \frac{f}{\varepsilon} \tag{4}$$

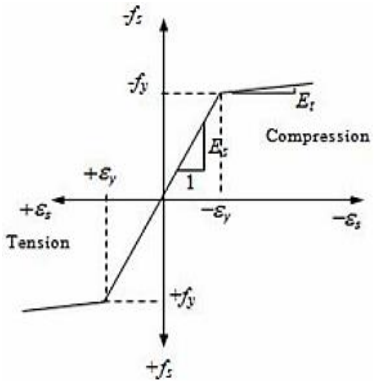

(a) Typical bilinear stress strain curve of steel

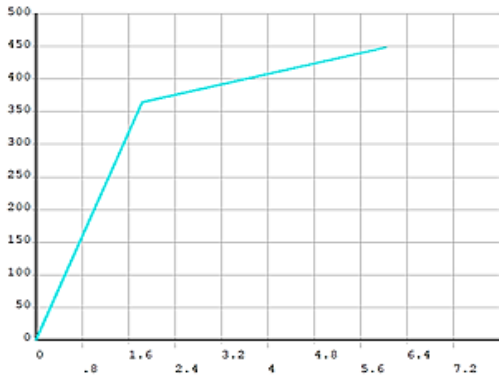

(b) Calculated stress strain curve for steel in ANSYS mechanical APDL (ANSYS User Manual Revision 18.0. 2018)

Fig. 4 Stress strain curves of steel

Where, E_c is elastic modulus of concrete, f_c' is compressive strength of concrete at 28 days in MPa, f is stress at any stain ε in MPa, ε is strain at stress (f), $\varepsilon_\circ$ is strain at ultimate compressive strength (f_c'). Typical shear transfer coefficients range from 0.0 to 1.0 with 1 representing rough cracks (no loss of shear transfer) and 0 representing smooth cracks (full loss of shear transfer) for concrete Kachlakev *et al*. (2001). Depending upon the strain hardening is considered or not, different researcher uses different stress strain relation model for FE modelling (Ayough *et al*. 2020). If strain hardening behaviour of steel is ignored, then elastic perfectly plastic model is most suited with yield plateau is infinity. However, in this research work, elastic linear hardening model is considered which considers linear strain hardening with slope equal to modulus of strain hardening. Fig. 4(a) shows the typical bilinear stress strain curve of steel. At starting, steel tube exhibits the linear elastic behaviour then shows strain hardening, stress increasing till facture occurs showing same behaviour in tension and compression as show in Fig. 4(b) developed in ANSYS mechanical APDL (ANSYS User Manual Revision 18.0. 2018).

2.2 Element type and meshing

SOLID65 is eight-node solid element, is used for 3-D modelling of solid with and without reinforcing bars which is most suitable for concrete models. SOLID65 has three degrees of freedom at each node, translational in nodal local axis X, Y and Z and has ability of cracking and crushing in three orthogonal directions. SOLID185 is used for 3-D modelling of steel tube having eight nodes with three degree of freedom UX, UY and UZ. It is suitable for prism, tetrahedral and pyramid shape for irregular regions. To perform the linear and nonlinear behavior of column, following Eqs. (5) and (6) shows the recommended element size for coarse and fine meshing Chou *et al*. (2000) and Baetu and Ciongradi (2011). The element meshing sizes of the CFST column are represented in Table 2.

$$\text{Element size of coarse mesh} = 0.049\ (\text{overall surface area of column})^{1/2} \quad (5)$$

$$\text{Element size of fine mesh} = 0.0245\ (\text{overall surface area of column})^{1/2} \quad (6)$$

Table 2 The meshing sizes of elements of CFST column

Element	Size
Concrete (SOLID65)	50 mm × 50 mm × 50 mm
Steel tube (SOLID185)	50 mm × 50 mm × 7.4 mm
Steel plates (SOLID185)	50 mm × 50 mm × 50 mm

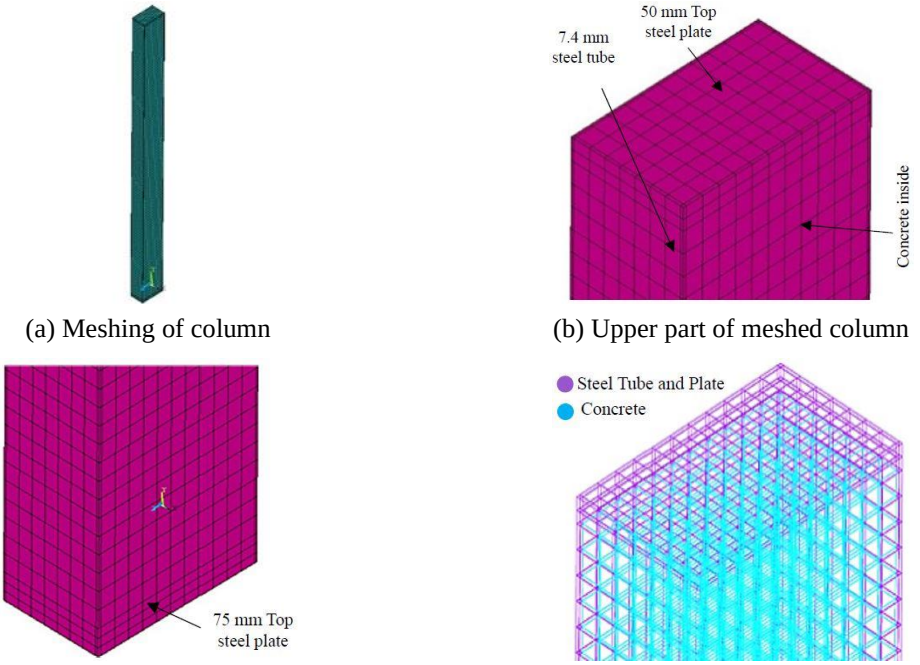

(a) Meshing of column (b) Upper part of meshed column

(c) Lower part of meshed column (d) Nodal connection of concrete and steel

Fig. 5 Element type and meshing details

The overall meshed CFST column shown in Fig. 5(a). 50 mm × 50 mm × 50 mm size of meshing for modelling of concrete, 50 mm × 50 mm × 7.4 mm meshing size for steel tube, width of element is 7.4 mm because thickness of steel tube is 7.4 mm and 50 mm × 50 mm × 50 mm size of meshing for steel plates at top and bottom of column as shown in Figs. 5(b) and 5(c). Perfect bond is considered in this study for simplifications. To provide perfect bond between concrete and steel, the nodes of concrete meshing must coincide with meshing nodes of the steel in such a way that two materials must share the same node as shown in Fig. 5(d).

2.3 Boundary condition and load

To ensure that the model is acting in the same way as experimental model, the boundary condition is needed to be applied at the required position as in experimental procedure. Fig. 6 shows the base of the column is fully constrained in translational displacement (UX, UY, UZ) and rotational displacement (ROTX, ROTY, ROTZ), and top end of column is allowed to move in translation displacement (UX, UY, UZ) and rotational displacement (ROTX, ROTY, ROTZ) as per

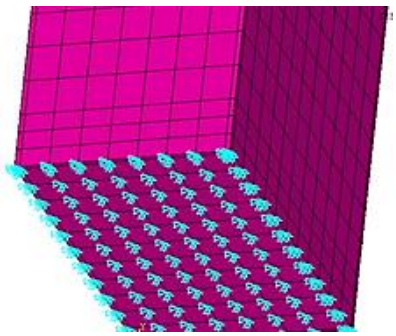

Fig. 6 Fully constrained support of column

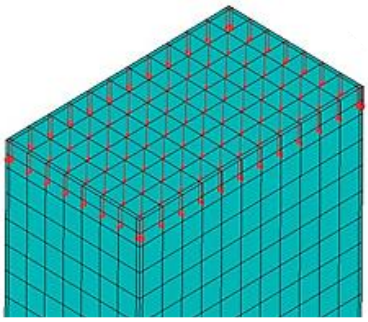

Fig. 7 Application of load

Perea *et al*. (2013). The gradual increasing and then decreasing cyclic load of 4349.4 kN is applied to CFST column to understand the behavior of column on top surface as shown in Fig. 7. To simulate the loading in FEA model, the loading is applied in term of sinusoidal function (limit $0 \rightarrow \pi$) as following

$$4349.4 \times \sin(0 \rightarrow \pi) \times Time \quad (7)$$

3. Verification of finite element method

3.1 Experimental results

Experimental investigations on concrete filled steel tube columns conducted by Perea *et al*. (2013) were used to validate the FEA model developed in this research work. Measured material properties and dimensions of tested specimen are summarized in Table 1.

3.2 Comparison of finite element results with experimental results

Table 3 shows the comparison of ultimate load and deflection at ultimate load between experiment and FEA model and found to be in good agreement with error of 1.71% and 4.54%, respectively. Load versus deflection curve of numerical model is also compared with experiment model.

Table 3 Comparison between FEA model and experimental model

Parameters	Experiment	FEA model	Difference
Ultimate load (*kN*)	4274	4349	1.71%
Deflection (*mm*)	174	166	4.54%

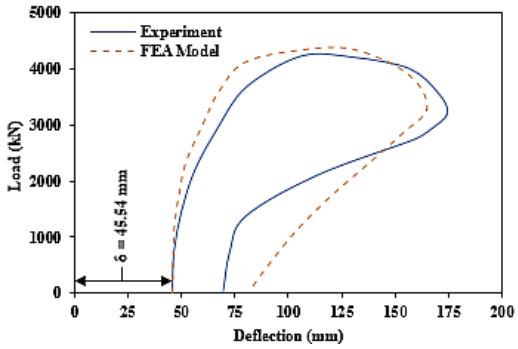

Fig. 8 Comparison of load-deflection curve of FEA model and experiment

Fig. 8 plots the load versus deflection curve for experiment and numerical model. At initial level at loading of 1000 kN, the experimental model and FEA model shows nearly same value of deflection, respectively, 48 mm and 46 mm width percentage difference of 4%. similarly, maximum difference of deflection during loading is found near about 4000 kN having values of 70 mm and 82 mm, respectively, with percentage difference of 14%. During the unloading of column, wide range of percentage difference of deflection found on load value of 3300 kN, 1200 kN and 0 kN in descending order are 5%, 30% and 14%, respectively. The deflection on load 3300 kN for experimental and FEA models are 165 *mm* and 174 mm. The deflection on load 1200 kN for experimental and FEA models are 74 mm and 105 mm. The deflection on load 0 kN for experimental and FEA models are 69 mm and 81 mm due to plastic behavior. FEA model efficiently predicted the ultimate load of column and load versus deflection curve against experiment.

After the application of maximum ultimate axial load, CFST column showed the deflection of 121 mm and overall deflection including δ is 166 mm (121 mm + 45.54 mm) as shown in Fig. 9(a). The value of 45.54 mm is the initial imperfection (δ) that is provided in column during modelling. Fig. 9(b) shows the stress distribution of concrete filled steel tube column under ultimate load. The red shaded area shows the maximum stress concentration where buckling is occurred and maximum tensile stresses with light blue shaded area are generated at opposite side of compressive stresses as shown in Fig. 9(b). The local buckling is occurred where compressive stress is maximum and maximum tensile stresses are generated at opposite side of compressive stresses where concrete cracking is occurred as shown in Fig. 8(b). With the application of ultimate load, steel tube starts buckling with concrete failure inside the steel tube. Fig. 10(a) shows the crushing and cracking pattern of the concrete in concrete filled steel tube at buckling location. Fig. 10(b) shows the close and side view of concrete failure inside steel tube. The green circles show the first crushing of concrete at the verge of failure of column and red circles represent the second crushing of the concrete that take place after the first crushing located at maximum compressive stress. The

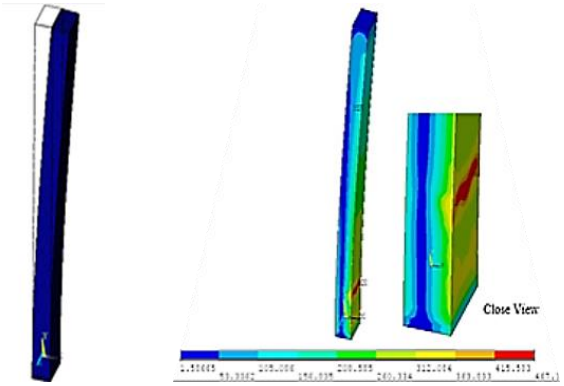

Fig. 9 Maximum deflection and stress distribution at peak / ultimate loading (left) Maximum deflection at ultimate load (right); (b) Stress distribution at ultimate load

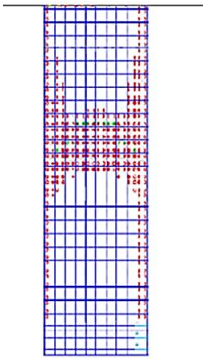

(a) Concrete failure pattern at buckling location

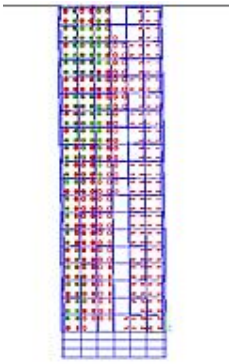

(b) Concrete compressive crushing and tensile cracking

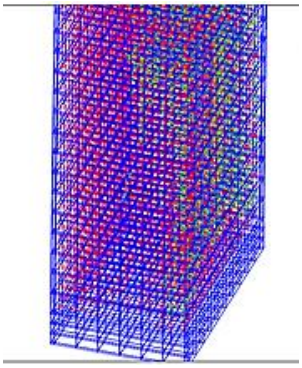

(c) Concrete 3D view failure pattern at buckling location

Fig. 10 Concrete failures

red lines located at the tensile stress face represents the tensile cracking of the concrete due to tensile stress at opposite side of compressive stresses. Fig. 10(c) represents the 3D view of concrete crushing and cracking inside the steel tube.

4. Parametric study and discussion

Total forty-two models were investigated for parametric study. Dimensions and materials properties of models are summarized in Table 4. Columns were divided into six groups with different parametric values. To calculate the effect of single parameter, the other parameters kept constant.

G1 group contains eight specimens, and each specimen has length (L) as a variable parameter. L-3.5, L-5.1, L-6.8 and L-8.5 are the intermediate columns having slenderness ratio between 50 to 200. L-9.0, L-9.4, L-10.0 and L-10.5 are the long columns having slenderness ratio more than 200. Initial imperfection (δ), thickness of steel tube (t), width (B), f_c' and f_y are kept constant to investigate the decrease in load carrying capacity of column by increasing the length of column.

G2 group contains eight specimens, and each specimen has initial imperfection (δ) as a variable parameter. δ-8, δ-16, δ-24, δ-32, δ-40, δ-64, δ-80, and δ-100 have initial imperfection (δ) from 8 mm to 100 mm to check the effect of initial imperfection (δ) on column. Length (L), thickness of steel tube (t), width (B), f_c' and f_y are kept constant to investigate the decrease in load carrying capacity of column by increasing the initial imperfection (δ).

G3 group contains six specimens, and each specimen has steel tube thickness (t) as a variable parameter. t-3, t-5, t-8, t-10, t-12, and t-15 have steel tube thickness (t) from 3 mm to 15 mm with the range of 4.12% to 23.45% of gross area of column. Length (L), initial imperfection (δ), width (B), f_c' and f_y are kept constant to investigate the increase in load carrying capacity of column by increasing the steel tube thickness (t).

G4 group contains six specimens, and each specimen has width (B) of column as a variable parameter. B-250, B-275, B-300, B-325, B-350, and B-375 have width (B) of column from 250 mm to 375 mm. Length (L), initial imperfection (δ), steel tube thickness (t), f_c' and f_y are kept constant to investigate the increase in load carrying capacity of column by increasing the width (B) of column.

G5 group contains eight specimens, and each specimen has compressive strength of concrete f_c' of column as a variable parameter: f_c'-20, f_c'-25, f_c'-35, f_c'-40, f_c'-52.5, f_c'-60, f_c'-70 and f_c'-87.6 have compressive strength of concrete from 20 MPa to 87.6 MPa. Length (L), initial imperfection (δ), steel tube thickness (t), f_c' and f_y are kept constant to investigate the increase in load carrying capacity of column by increasing the compressive strength of concrete f_c' of column. G6 group contains six specimens, and each specimen has yield strength of steel F_y of column as a variable parameter. f_y-75, f_y-150, f_y-200, f_y-250, f_y-300, and f_y-370 have yield strength of steel f_y from 75 MPa to 370 MPa. Length (L), initial imperfection (δ), steel tube thickness (t), width (B) and f_c' are kept constant to investigate the increase in load carrying capacity of column by increasing the yield strength of steel f_y.

The specimen codes are explained as L-3.5 is L stand for column variable such as length and 3.5 is value of variable. δ-8: δ stand for column initial imperfection and 8 is value of δ. t-3 is stand for steel tube thickness and 3 is the value of thickness (t). B-250 is stand for width of column and 250 is value of width (B). f_c'-20 is stand for concrete compressive strength and 20 is value of concrete compressive strength. f_y-75 is stand for steel strength and 75 is value of steel strength of steel tube and steel plate.

Forty two columns were modeled in ANSYS (ANSYS User Manual Revision 18.0. 2018) software to verify the accuracy of results of ANSYS with proposed equation results as shown in

Table 4 Specimen dimensions and material properties for parametric study

Group	Specimen code	Remarks	L (mm)	δ (mm)	t (mm)	B (mm)	f_c' (MPa)	f_y (MPa)
G1	L-3.5	Intermediate column	3500	48	8	300	52.5	220
	L-5.1	Intermediate column	5100	48	8	300	52.5	220
	L-6.8	Intermediate column	6800	48	8	300	52.5	220
	L-8.5	Intermediate column	8500	48	8	300	52.5	220
	L-9.0	Long column	9000	48	8	300	52.5	220
	L-9.4	Long column	9400	48	8	300	52.5	220
	L-10.0	Long column	10000	48	8	300	52.5	220
	L-10.5	Long column	10500	48	8	300	52.5	220
G2	δ-8		7000	8	8	300	52.5	220
	δ -16		7000	16	8	300	52.5	220
	δ -24		7000	24	8	300	52.5	220
	δ -32		7000	32	8	300	52.5	220
	δ -40		7000	40	8	300	52.5	220
	δ -64		7000	64	8	300	52.5	220
	δ -80		7000	80	8	300	52.5	220
	δ -100		7000	100	8	300	52.5	220
G3	t-3	Steel ratio is 4.12 to 23.45%	7000	48	3	300	52.5	220
	t-5		7000	48	5	300	52.5	220
	t-8		7000	48	8	300	52.5	220
	t-10		7000	48	10	300	52.5	220
	t-12		7000	48	12	300	52.5	220
	t-15		7000	48	15	300	52.5	220
G4	B-250		7000	48	8	250	52.5	220
	B-275		7000	48	8	275	52.5	220
	B-300		7000	48	8	300	52.5	220
	B-325		7000	48	8	325	52.5	220
	B-350		7000	48	8	350	52.5	220
	B-375		7000	48	8	375	52.5	220
G5	f_c'-20	Normal strength concrete	7000	48	8	300	20	220
	f_c'-25		7000	48	8	300	25	220
	f_c'-35		7000	48	8	300	35	220
	f_c'-40		7000	48	8	300	40	220
	f_c'-52.5	High strength concrete	7000	48	8	300	52.5	220
	f_c'-60		7000	48	8	300	60	220
	f_c'-70		7000	48	8	300	70	220
	f_c'-87.6		7000	48	8	300	87.6	220

Table 4 Continued

G6	f_y-75	7000	48	8	300	52.5	75
	f_y-150	7000	48	8	300	52.5	150
	f_y-200	7000	48	8	300	52.5	200
	f_y-250	7000	48	8	300	52.5	250
	f_y-300	7000	48	8	300	52.5	300
	f_y-370	7000	48	5	300	52.5	370

Table 5 Axial load capacities with and without δ from FE models

Dimensions				Material properties		Load capacity		
δ (mm)	L (mm)	B (mm)	t (mm)	f_c' (MPa)	f_y (MPa)	U (kN)	U' (kN)	U/U' (α)
0	7000	300	8	52.5	220	4366	4366	1
8	7000	300	8	52.5	220	3514.01	4366	0.8048
16	7000	300	8	52.5	220	3003.15	4366	0.6878
24	7000	300	8	52.5	220	2635.40	4366	0.6036
32	7000	300	8	52.5	220	2345.45	4366	0.5372
40	7000	300	8	52.5	220	2145.14	4366	0.4913
64	7000	300	8	52.5	220	1655.85	4366	0.3792
80	7000	300	8	52.5	220	1385.06	4366	0.3172
100	7000	300	8	52.5	220	1101.58	4366	0.2523

Table 5.

4.1 Effect of length

Fig. 11 shows the load carrying capacity of column with increase of length of column. The ductility of columns increased as KL/r of columns increases but load carrying capacity of columns decreased because of increase in length of columns from intermediate column to long column.

L-3.5 and L-5.1 failed at very high load and less deflection due to high stiffness because of very less KL/r nearly close to short column but still categorized in intermediate columns and vice versa. L-9, L-9.4, L-10 and L-10.5 showed failure at very large deflection but very less load due to very high ductility and low stiffness of column. The reduction load carrying capacity of L-3.5 and L-5.1 by increasing the length are almost same up to 500 kN with same deflection value of 52 mm due to elastic range and failed at 2717 kN and 2256 kN with deflection of 78 mm and 105 mm, respectively. Similarly, the reduction in load carrying capacity of L-10, L-10.5 by increasing length are almost same up to 350 kN with deflection of 61 mm due to large slenderness ratio and more ductile behavior and failed at 1091 kN and 1009 kN as shown in Fig. 11.

The load carrying capacity of CFST column linearly decreased with the increase in length of column because the most suited trendline for load versus length is linear as shown in Fig. 12. This helped to decide for selection of type of regression analysis. Difference between the highest and lowest capacity is 67.48% which shows that reduction in capacity is 272 N/mm.

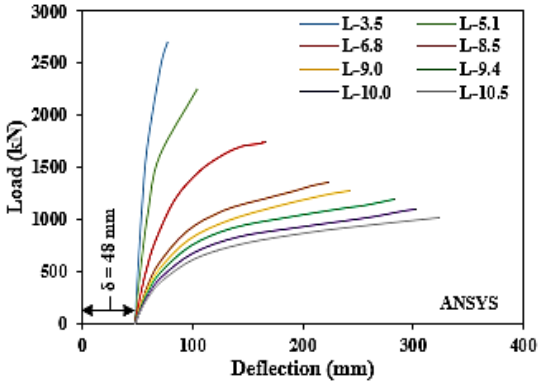

Fig. 11 Load versus deflection curve (*Variable* = *L*)

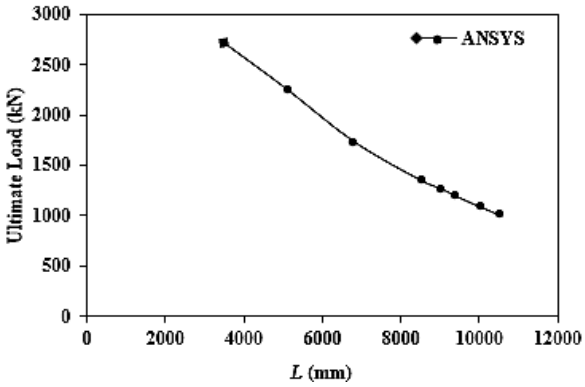

Fig. 12 Ultimate Load versus L

4.2 Effect of initial imperfection

In this section, the effect of various initial imperfection (δ) of CFST column is investigated. Fig. 13 shows that δ-8 and δ-24 gave the highest load capacity of 3414 kN and 3003 kN with very less deflection of 20 mm and 39 mm, respectively. δ-64 and δ-100 mm gave capacity of 1385 kN and 1101 kN with very high deflection of 230 mm and 242 mm. The graph shows that axial load carrying capacity of columns decrease and deflection at failure load increase as (δ) increases. Because of P-δ effect, as (δ) in column increases, the eccentricity in column with respect to column axial load axial load increase. Due to this reason, the large moment magnification developed in column which causes the reduction in capacity as shown in Fig. 14.

Fig. 14 shows that load carrying capacity of the CFST column decreases exponentially with increase of initial imperfection (δ). Load carrying capacity when initial imperfection (δ) is 8 mm is 3414 kN which is exponentially decreased to 1101 kN having initial imperfection (δ) of 100 mm.

4.3 Effect of steel tube thickness

Fig. 15 shows that t-3 column provides less confinement effect as compare to t-5, t-8 t-10, t-12, t-15 columns because stress bearing capacity of t-3 having steel tube thickness 3 mm column is

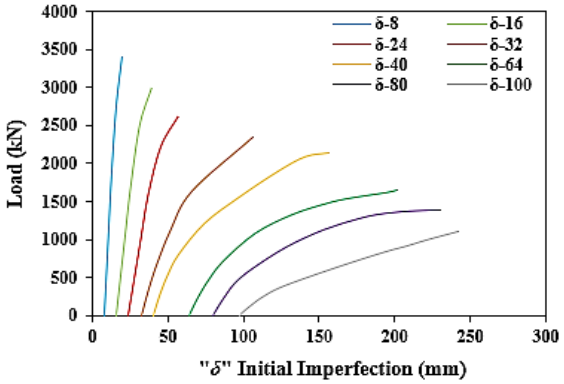

Fig. 13 Load versus deflection curve (*Variable* = δ)

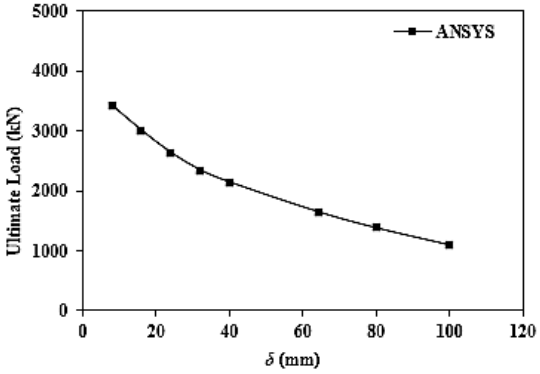

Fig. 14 Ultimate load versus δ

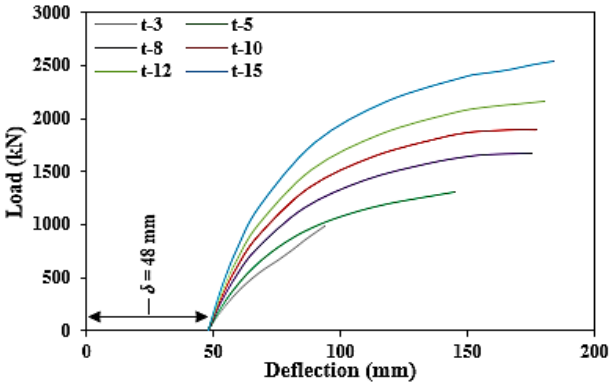

Fig. 15 Load versus deflection curve (Variable = t)

much lesser than t-5, t-8, t-10, t-12 and t-15 having steel tube thickness of 8 mm, 10 mm, 12 mm and 15 mm. t-8, t-10, t-12 and t-15 have very less difference in deflection value of 175 mm, 177 mm, 180 mm and 184 mm but load carrying capacity is increased to large difference due to confinement effect of steel tube with the value of 1669 kN, 1896 kN, 2163 kN and 2545 kN,

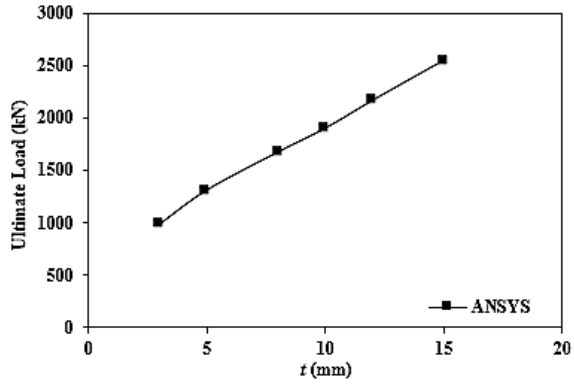

Fig. 16 Ultimate load versus *t*

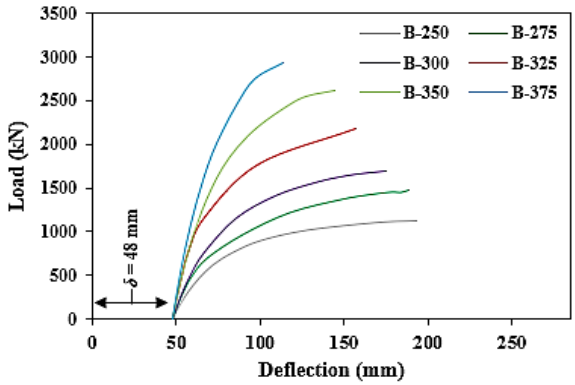

Fig. 17 Load versus deflection curve (Variable = B)

respectively as shown in Fig. 14. The ultimate load carrying capacity of CFST columns (*t-5*, *t-8*, *t-10*, *t-12 and t-15*) against steel tube thickness (t) is shown in Fig. 16.

Ultimate load carrying capacity of column having steel tube thickness 3 mm (t-3) is 980 kN which is linearly increased to 2546 kN having thickness of steel tube 15 mm (t-15) by increasing the thickness of steel tube.

4.4 Effect of width

Six different values of width (B) of column are selected to investigate the loading strength and ductility of column with the increase in size of column. Fig. 17 shows that B-250, B-275, B-300, B-325, B-350 and B-375 failed at high load of 1118 kN, 1471 kN, 1698 kN, 2176 kN, 2612 kN and 2925 kN with decreasing value of deflections of 193 mm, 188 mm, 175 mm, 156 mm, 144 mm and 113 mm, respectively which shows that by increasing the size of columns, the ductility of column decreases, and stiffness of column increases. This phenomenon gradually changes in descending order as shown in Fig. 17.

The ultimate load carrying capacity of CFST columns (B-*250*, *B-275*, *B-300*, *B-325*, *B-350 and B-375*) against width of column (B) is shown in Fig. 18. Ultimate load carrying capacity of column having width 250 mm (B-250) is 1118 kN which is linearly increased to 2975 kN having width

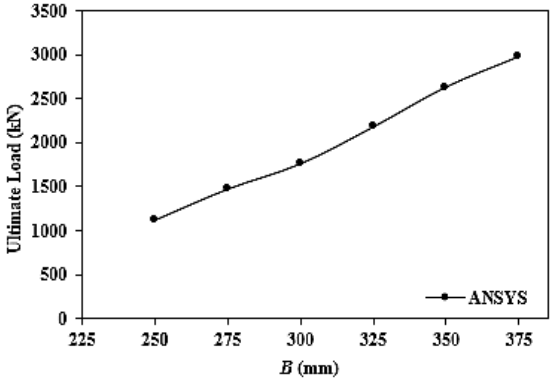

Fig. 18 Ultimate load versus *B*

375 mm (B-375) by increasing the width of column.

4.5 Effect of compressive strength of concrete

To assess the behavior of CFST column under different compressive strength of concrete (f_c'), the eight different values of compressive strength of concrete (f_c') are selected with normal and high strength concrete. f_c'-20, f_c'-25, f_c'-35 and f_c'-40 have normal strength concrete (NSC). f_c'-52.5, f_c'-60, f_c'-70, f_c'-87.6 have high strength concrete (HSC). All the FEA models have the same load carrying capacity and deflection up to 500 kN load. Fig. 19 shows that f_c'-20 and f_c'-87.6 have the load carrying capacity of column of 1329 kN and 2152 kN with almost same deflection value of 159 mm and 160 mm, respectively. Similar behavior is observed in f_c'-25, f_c'-35, f_c'-40, f_c'-52.5, f_c'-60 and f_c'-70. As the compressive strength of concrete (f_c') of columns increases, axial load carrying capacity of column increases because of increased compressive strength with slightly larger deflection at ultimate load.

The ultimate load carrying capacity of CFST columns (f_c'-20, f_c'-25, f_c'-35, f_c'-40, f_c'-52.5, f_c'-60, f_c'-70, f_c'-87.6) against compressive strength of column (f_c') is shown in Fig. 20. Ultimate load carrying capacity of column having compressive strength of 20 MPa (f_c'-20) is 1392 kN which is linearly increased to 2152 kN having compressive strength of 87.6 MPa (f_c'-87.6) by increasing the compressive strength of column.

4.6 Effect of steel tube strength

Eight different values of strength of steel tube (f_y) are selected to understand the effect to steel tube strength. f_y-75 and f_y-150 failed at load of 1338 kN and 1138 kN with deflection value of 98 mm and 120 mm, respectively showed less confinement effect and ductility of column, this is reason of decreased load carrying capacity of column. f_y-200, f_y-250, f_y-300 and f_y-370 failed at very close value of loads 1663 kN, 1718 kN, 1815 kN and 1867 kN with deflections of 189 mm, 191 mm, 204 mm and 236 mm, respectively shows that as the load carrying capacity of column is slightly increasing with increase of strength of steel tube increases but shows no significant change in ductility of columns with also remain same as shown in Fig. 21.

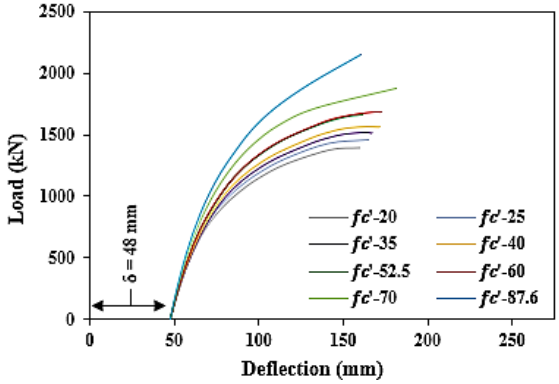

Fig. 19 Load versus deflection curve (Variable = f_c')

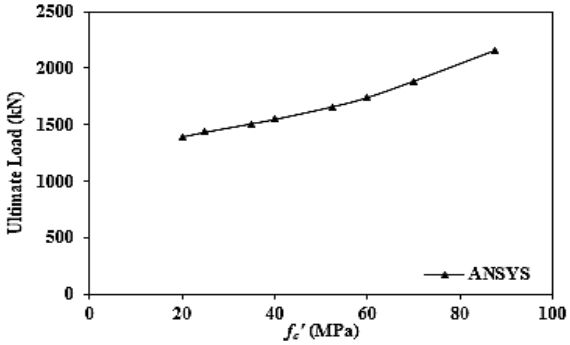

Fig. 20 Ultimate load versus f_c'

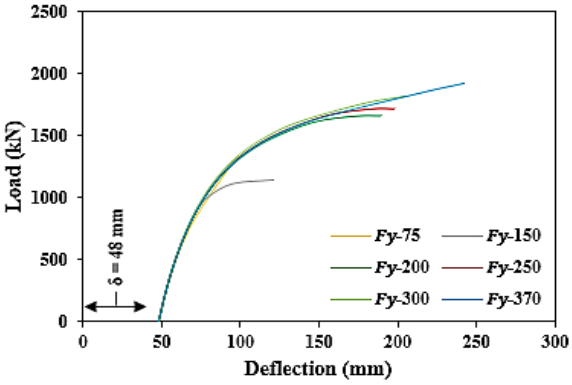

Fig. 21 Load versus deflection curve (Variable = f_y)

The ultimate load carrying capacity of CFST columns (f_y-75, f_y-150, f_y-200, f_y-250, f_y-300, f_y-370) against yield strength of steel tube (f_y) is shown in Fig. 22. It can be seen that ultimate load carrying capacity of column having yield strength of steel of 75 MPa (f_y-75) is 1338 kN which is linearly increased to 1926 kN having yield strength of steel tube of 370 MPa (f_y-370) by

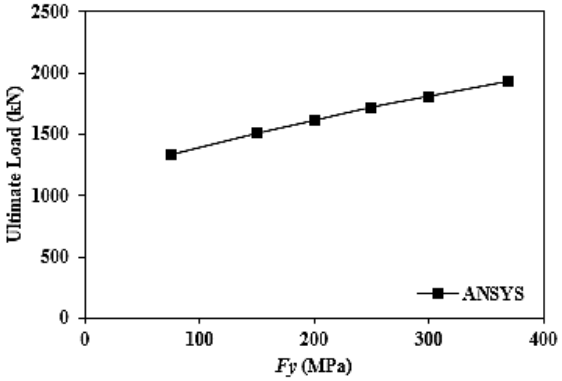

Fig. 22 Ultimate load versus f_y

increasing the yield strength of steel tube. Graph shows increase in capacity of column with the increase of strength of steel tube (f_y). steel tube strength shows the minor enhancement in increase in overall load capacity of column and concrete shows the large contribution to loading capacity.

5. Empirical equation

Generalized empirical equation is developed from forty-two FEA model by performing multiple linear regression analysis on linear responded variables (L, B, t, f_c', F_y). Empirical equation can predict the axial load carrying capacity (U°) of CFST column by putting the value of variables without including the initial imperfection (δ) (out of straightness) because initial imperfection (δ) shows the nonlinear behavior and multiplying strength reduction coefficient (φ) corresponding to δ value to obtain the reduced axial load carrying capacity (U_e) of column.

$$U° = -0.451L + 306.36t + 34.195B + 35.267f_c' + 4.456f_y - 8376.67 \quad (8)$$

Where U° is pure axial ultimate load capacity without δ in kN, L is length in mm, t is thickness of steel tube in mm, B is width of column in mm, f_c' is compressive strength of concrete in MPa and f_y is steel strength in MPa.

5.1 Reduction factor (φ)

The reduction in axial load carrying capacity (U_e) due to initial imperfection (δ) is calculated by reduction coefficient (φ) which is calculated by nonlinear trend of graph between (U/U′) called as α, where U is axial load capacity calculated from ANSYS models including initial imperfection (δ) and U′ is axial load capacity calculated from ANSYS models without initial imperfection (δ). Table 5 summarized the ultimate load capacities with δ and without δ. By multiplying the reduction factor (φ) to pure axial capacity (U°) of column, the reduced axial load carrying capacity (U_e) can be achieved. The Eq. (9) is developed by adopting most suited function of curve which is plotted between α and δ as show in Fig. 23. The most suited function of below curve which gives most close results with the value of *R* square of 0.998 and maximum error of 0.0238 is following as

$$\varphi = 0.952^{(\delta^{0.722})} \tag{9}$$

$$U_e = \varphi \times U^{o} \tag{10}$$

Where φ is reduction factor, δ is initial imperfection, U^o is axial load capacity calculated from Eq. (8) without δ, U_e is axial load capacity including δ calculated from Eq. (10).

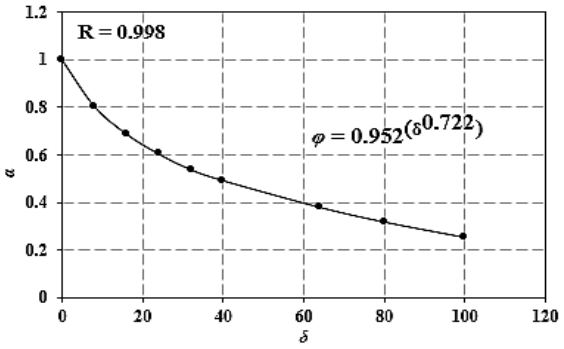

Fig. 23 α versus δ

Table 6 Comparison of load carrying capacity obtained from parametric study and equation

Group	Specimen	U_{ANSYS}	U_e	$\frac{U_{ANSYS}}{U_e}$	SD (CoV [%])
G1	*L-3.5*	2717	2496.49	1.088	0.07 (6.93)
	L-5.1	2256.5	2173.22	1.038	
	L-6.8	1738	1829.75	0.949	
	L-8.5	1353.50	1486.27	0.910	
	L-9.0	1273.18	1385.25	0.919	
	L-9.4	1196	1304.43	0.916	
	L-10.0	1091.05	1183.21	0.922	
	L-10.5	1009	1082.19	0.932	
G2	*δ-8*	3514	3209.07	1.095	0.01 (0.93)
	δ -16	3003.15	2780.43	1.080	
	δ -24	2635.4	2456.57	1.072	
	δ -32	2345.45	2194.86	1.068	
	δ -40	2145.14	1976.09	1.085	
	δ -64	1625.85	1485.92	1.094	
	δ -80	1365.06	1249.63	1.092	
	δ -100	1101.58	1019.57	1.080	

Table 6 Continued

Group	Specimen	U_{ANSYS}	U_e	$\frac{U_{ANSYS}}{U_e}$	SD (CoV [%])
G3	*t-3*	990.86	1104.41	0.897	0.02 (1.78)
	t-5	1306.15	1378.38	0.947	
	t-8	1669.14	1789.34	0.932	
	t-10	1896.54	2063.31	0.919	
	t-12	2163.43	2337.28	0.925	
	t-15	2546.51	2748.24	0.926	
G4	*B-250*	1118.90	1024.84	1.091	0.04 (3.71)
	B-275	1471	1407.09	1.045	
	B-300	1758.5	1789.34	0.982	
	B-325	2176.41	2171.59	1.002	
	B-350	2630.12	2553.84	1.029	
	B-375	2975.9	2936.09	1.013	
G5	f_c'*-20*	1392.91	1276.83	1.090	0.07 (7.20)
	f_c'*-25*	1435.34	1355.68	1.058	
	f_c'*-35*	1508.8	1513.37	0.996	
	f_c'*-40*	1547.5	1592.22	0.971	
	f_c'*-52.5*	1658	1789.34	0.926	
	f_c'*-60*	1738.73	1907.61	0.911	
	f_c'*-70*	1882	2065.31	0.911	
	f_c'*-87.6*	2152.5	2342.85	0.918	
G6	f_y*-75*	1358.16	1500.38	0.905	0.01 (0.96)
	f_y*-150*	1507.9	1649.84	0.913	
	f_y*-200*	1611.77	1749.48	0.921	
	f_y*-250*	1718	1849.12	0.929	
	f_y*-300*	1805.37	1948.76	0.926	
	f_y*-75*	1926.37	2088.26	0.922	

5.2 Comparison of (U_e) results with ANSYS results

Forty-two columns are modeled in ANSYS (ANSYS User Manual Revision 18.0. 2018) software to verify the accuracy of results of ANSYS with proposed equation results as shown in Table 6. SD and CoV stand for standard deviation and coefficient of variation respectively. The

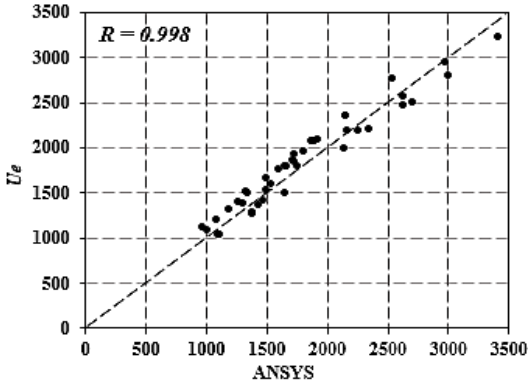

Fig. 24 U_e result versus ANSYS result

maximum value of SD and CoV are 0.07 and 7.20% which are less then maximum allowed value of 15%. It shows that maximum values of $\frac{U_{ANSYS}}{U_e}$ lies about mean values.

Axial capacities (U_e) calculated from Eq. (10) are compared with ANSYS models as shown in Fig. 24. The deviation of points of graph between ANSYS results and U_e results on 45° inclined line on graph is not too much dispersed with maximum error of 9% between U_e and ANSYS which shows reliable results comparison.

6. Limitations

Friction effect is not considered between concrete and steel tube.

One end fixed and one end free boundary condition is considered for research purpose.

Square concrete filled steel tube column is considered for this research work.

Time dependent nonlinearities that may include temperature, creep and shrinkage are not included in this study.

7. Conclusions

The FEA modelling of CFST column in ANSYS is conducted to synchronize the experimental results. The effect of different parameters during FEA modelling is evaluated. The main purpose is to develop relationship related to initial imperfection (δ) of column that can predict the reduced axial load carrying capacity (U_e) of column as initial imperfection (δ) increases.

- The FEA modelling shows the efficient comparison against the experimental work that provides the reliability of FEA procedure. Moreover, modelling and convergence of solution of concrete is difficult in ANSYS because of its brittle property.
- With the parametric study of geometric parameters (L, t, B) and material properties (f_c', f_y), Eq. (8) is derived which can be used to axial load carrying capacity of column without initial imperfection. Eq. (9) is derived from the parametric study of different initial imperfection value (δ-8, δ -16, δ -24, δ -32, δ -40, δ -64, δ -80, δ -100) which is called as Reduction Factor

(φ) which can be multiply with Eq. (8) to get reduced axial load carrying capacity of column Eq. (10).

- Combined use of Eq. (8), Eq. (9) and Eq. (10) shows the reliable results against results of ANSYS with the maximum error of only 9% which shows that empirical relationship can predict much accurate results.
- Set of empirical equations Eq. (8), Eq. (9) and Eq. (10) can be used for predicting the early estimation of axial capacity of CFST column. Furthermore, it can also be used for predicting loading capacity which is out of range of loading capacity of machine.
- By increasing the strength of steel tube, the axial load carrying capacity of steel tube is slightly increasing but has no significant effect on ductility of column with the increase in strength of steel tube.

Acknowledgments

The authors are grateful to staff of Structural Engineering Division of Civil Engineering Department at National University of Computer and Emerging Sciences, Lahore, Pakistan for providing us valuable guidance related FEA modelling.

References

ANSYS User Manual Revision 18.0. (2018), ANSYS Inc., Canonburg, PA, USA.

Ayough, P., Sulong, N.R. and Ibrahim, Z. (2020), "Analysis and review of concrete-filled double skin steel tubes under compression", *Thin-Wall. Struct.*, **148**, 106495. https://doi.org/10.1016/j.tws.2019.106495

Ayough, P., Ibrahim, Z., Sulong, N.R. and Hsiao, P.-C. (2021), "The effects of cross-sectional shapes on the axial performance of concrete-filled steel tube columns", *J. Constr. Steel Res.*, **176**, 106424. https://doi.org/10.1016/j.jcsr.2020.106424

Baetu, S. and Ciongradi, I.-P. (2011), "Nonlinear finite element analysis of reinforced concrete slit walls with ANSYS (I)", *Buletinul Institutului Politehnic din lasi, Sectia Constructii, Arhitectura*, **57**(1), 31.

Belal, M.F., Mohamed, H.M. and Morad, S.A. (2015), "Behavior of reinforced concrete columns strengthened by steel jacket", *HBRC Journal*, **11**(2), 201-212. https://doi.org/10.1016/j.hbrcj.2014.05.002

Cai, J., Pan, J., Lu, C. and Li, X. (2020), "Nonlinear analysis of circular concrete-filled steel tube columns under eccentric loading", *Magaz. Concrete Res.*, **72**(6), 292-303. https://doi.org/10.1680/jmacr.18.00204

Chou, S., Chai, G. and Ling, L. (2000), "Finite element technique for design of stub columns", *Thin-Wall. Struct.*, **37**(2), 97-112. https://doi.org/10.1016/S0263-8231(00)00018-5

Du, G., Babic, M., Wu, F., Zeng, X. and Bie, X.-M. (2019), "Experimental and numerical studies on concrete filled circular steel tubular (CFCST) members under impact loads", *Int. J. Civil Eng.*, **17**(8), 1211-1226. https://doi.org/10.1007/s40999-018-0379-8

Effendi, M.K. (2020), "The effect of concrete-steel interface model on finite element analysis of concrete filled square steel tube beam", *Civil Engineering Journal*, **1**(2), 135-146. https://doi.org/10.14311/CEJ.2020.02.0012

Ellobody, E., Young, B. and Lam, D. (2006), "Behavior of normal and high strength concrete-filled compact steel tube circular stub columns", *J. Constr. Steel Res.*, **62**(7), 706-715. https://doi.org/10.1016/j.jcsr.2005.11.002

Fang, H. and Visintin, P. (2022), "Structural performance of geopolymer-concrete-filled steel tube members subjected to compression and bending", *J. Constr. Steel Res.*, **188**, 107026. https://doi.org/10.1016/j.jcsr.2021.107026

Gupta, P., Khaudhair, Z.A. and Ahuja, A. (2012), "A study on load carrying capacity and behavior of concrete filled steel tubular members subjected to axial compression", *Proceedings of the 11th International Conference on Concrete Engineering and Technology*, Putrajaya, Malaysia, June.

He, L., Lin, S. and Jiang, H. (2019), "Confinement effect of concrete-filled steel tube columns with infill concrete of different strength grades", *Frontiers Mater*., **6**, p. 71. https://doi.org/10.3389/fmats.2019.00071

Hernández-Figueirido, D., Romero, M., Bonet, J. and Montalvá, J. (2012), "Ultimate capacity of rectangular concrete-filled steel tubular columns under unequal load eccentricities", *J. Constr. Steel Res*., **68**(1), 107-117. https://doi.org/10.1016/j.jcsr.2011.07.014

Hossain, K., Chu, K. and Anwar, M.S. (2021), "Axial load behavior of ultrahigh strength concrete-filled steel tube columns of various geometric and reinforcement configurations", *Infrastructures*, **6**(5), p. 66. https://doi.org/10.3390/infrastructures6050066

Hu, H.-T., Huang, C.-S., Wu, M.-H. and Wu, Y.-M. (2003), "Nonlinear analysis of axially loaded concrete-filled tube columns with confinement effect", *J. Struct. Eng*., **129**(10), 1322-1329. https://doi.org/10.1061/(ASCE)0733-9445(2003)129:10(1322)

Jin, L., Chen, H., Fan, L., Li, P. and Du, X. (2020), "Size Effect on Nominal Strength of Lightweight and Normal Concrete-Filled Steel Tube Columns under Axial Compression: Mesoscale Simulations", *J. Struct. Eng*., **146**(12), 04020265. https://doi.org/10.1061/(ASCE)ST.1943-541X.0002827

Kachlakev, D., Miller, T., Yim, S., Chansawat, K. and Potisuk, T. (2001), "Finite element modeling of reinforced concrete structures strengthened with FRP laminates", Ph.D.; California Polytechnic State University, Oregon State University, Corvallis, OR, USA.

Lakshmi, B. and Shanmugam, N. (2002), "Nonlinear analysis of in-filled steel-concrete composite columns", *J. Struct. Eng*., **128**(7), 922-933. https://doi.org/10.1061/(ASCE)0733-9445(2002)128:7(922)

Li, P., Zhang, T. and Wang, C. (2018), "Behavior of concrete-filled steel tube columns subjected to axial compression", *Adv. Mater. Sci. Eng*., 2018. https://doi.org/10.1155/2018/4059675

Liang, Q.Q., Uy, B. and Liew, J. (2007), "Strength of concrete-filled steel box columns with buckling effects", *Austral. J. Struct. Eng*., **7**(2), 145-155. https://doi.org/10.1080/13287982.2007.11464972

Liu, X., Liu, J., Yang, Y., Cheng, G. and Lanning, J. (2020), "Resistance of special-shaped concrete-filled steel tube columns under compression and bending", *J. Constr. Steel Res*., **169**, 106038. https://doi.org/10.1016/j.jcsr.2020.106038

Lu, F., Li, S. and Sun, G. (2007), "A study on the behavior of eccentrically compressed square concrete-filled steel tube columns", *J. Constr. Steel Res*., **63**(7), 941-948. https://doi.org/10.1016/j.jcsr.2006.09.003

Nguyen, D.H., Hong, W.-K., Ko, H.-J. and Kim, S.-K. (2019), "Finite element model for the interface between steel and concrete of CFST (concrete-filled steel tube)", *Eng. Struct*., **185**, 141-158. https://doi.org/10.1016/j.engstruct.2019.01.068

Nour, A.I. and Güneyisi, E.M. (2019), "Prediction model on compressive strength of recycled aggregate concrete filled steel tube columns", *Compos. Part B*: *Eng*., **173**, 106938. https://doi.org/10.1016/j.compositesb.2019.106938

Patel, V.I., Liang, Q.Q. and Hadi, M.N. (2017), "Nonlinear analysis of circular high strength concrete-filled stainless steel tubular slender beam-columns", *Eng. Struct*., **130**, 1-13. https://doi.org/10.1016/j.engstruct.2016.10.004

Perea, T., Leon, R.T., Hajjar, J.F. and Denavit, M.D. (2013), "Full-scale tests of slender concrete-filled tubes: axial behavior", *J. Struct. Eng*., **139**(7), 1249-1262. https://doi.org/10.1061/(ASCE)ST.1943-541X.0000784

Portolés, J., Romero, M.L., Bonet, J. and Filippou, F. (2011a), "Experimental study of high strength concrete-filled circular tubular columns under eccentric loading", *J. Constr. Steel Res*., **67**(4), 623-633. https://doi.org/10.1016/j.jcsr.2010.11.017

Portolés, J., Romero, M.L., Filippou, F.C. and Bonet, J. (2011b), "Simulation and design recommendations of eccentrically loaded slender concrete-filled tubular columns", *Eng. Struct*., **33**(5), 1576-1593. https://doi.org/10.1016/j.engstruct.2011.01.028

Sakino, K., Nakahara, H., Morino, S. and Nishiyama, I. (2004), "Behavior of centrally loaded concrete-filled steel-tube short columns", *J. Struct. Eng.*, **130**(2), 180-188. https://doi.org/10.1061/(ASCE)0733-9445(2004)130:2(180)

Schneider, S.P. (1998), "Axially loaded concrete-filled steel tubes", *J. Struct. Eng.*, **124**(10), 1125-1138. https://doi.org/10.1061/(ASCE)0733-9445(1998)124:10(1125)

Song, T.-Y. and Xiang, K. (2020), "Performance of axially-loaded concrete-filled steel tubular circular columns using ultra-high strength concrete", *Structures*, **24**, 163-176. https://doi.org/10.1016/j.istruc.2019.12.019

Varma, A.H., Ricles, J.M., Sause, R. and Lu, L.-W. (2002), "Experimental behavior of high strength square concrete-filled steel tube beam-columns", *J. Struct. Eng.*, **128**(3), 309-318. https://doi.org/10.1061/(ASCE)0733-9445(2002)128:3(309)

Wang, Y.Z. and Li, B.S. (2013), "Finite element analysis for concrete filled double-skin steel tubular stub columns", *Adv. Mater. Res.*, **690**, 696-699. https://doi.org/10.4028/www.scientific.net/AMR.690-693.696

Wei, J., Luo, X., Lai, Z. and Varma, A.H. (2020), "Experimental behavior and design of high-strength circular concrete-filled steel tube short columns", *J. Struct. Eng.*, **146**(1), 04019184. https://doi.org/10.1061/(ASCE)ST.1943-541X.0002474

Yu, M., Zha, X., Ye, J. and She, C. (2010), "A unified formulation for hollow and solid concrete-filled steel tube columns under axial compression", *Eng. Struct.*, **32**(4), 1046-1053. https://doi.org/10.1016/j.engstruct.2009.12.031

Yu, M., Zha, X., Ye, J. and Li, Y. (2013), "A unified formulation for circle and polygon concrete-filled steel tube columns under axial compression", *Eng. Struct.*, **49**, 1-10. https://doi.org/10.1016/j.engstruct.2012.10.018

CC